Concerted versus stepwise proton transfer reactions in the [2, 2'-bipyridyl]-3-3'-diol molecule: A static and dynamic ab-initio investigation

Lorenzo Briccolani-bandini, Eric Brémond, Marco Pagliai, Gianni Cardini, Ilaria Ciofini, Carlo Adamo

Concerted vs. Stepwise Proton Transfer reactions in the [2, 2'-bipyridyl]-3-3'-diol molecule : a static and dynamic ab-initio investigation

Lorenzo Briccolani-Bandini[a], Eric Brémond[b], Marco Pagliai[a], Gianni Cardini[a], Ilaria Ciofini[c] and Carlo Adamo[c,d]

a) Dipartimento di Chimica "Ugo Schiff", Università degli Studi di Firenze, Via della Lastruccia 3, 50019 Sesto Fiorentino, Italy; b) Université Paris Cité, ITODYS, CNRS, F-75006 Paris, France; c) Chimie ParisTech, PSL University, CNRS, I-CLeHS, UMR 8060 Institute of Chemistry for Health and Life Sciences, F-75005 Paris, France, d) Institut Universitaire de France, 103 Boulevard Saint Michel, F-75005 Paris, France

Abstract

The double proton transfer (PT) reaction has been investigated in the [2,2'-bipyridyl]-3-3'-diol, a complex molecule where the proton movements is coupled to significant rearrangement of the electronic structure. Moreover, the reaction could be concerted, that is the two protons are exchanged simultaneously, or stepwise, where the two protons are transferred sequentially. To this end, a static exploration of the potential energy surface (PES) was carried together with the analysis of the Free-Energy Surface (FES), both surfaces being evaluated at Density Functional Theory (DFT) level and different exchange-correlation functionals. While the concerted mechanism has been clearly discharged, the characteristics of the stepwise PT significantly depends on the chosen functionals, some suggesting a clear stepwise mechanism characterized by a stable reaction intermediates and two transitions states, whereas other approaches propend for a asynchronous PT, with a single TS. These features appear on both PES and FES, albeit some differences appears dut to their different nature.

Keywords : DFT, Ab Initio Molecular Dynamics, Proton Transfer, Free Energy Surface

1.Introduction

Proton Transfer (PT) processes are ubiquitous in Chemistry, having a central role for a large number of different chemical systems, from those of interest in biology, to material science, to astrochemistry and catalysis[1]. Despite the simple reaction mechanism, roughly a proton moving from a donor to an acceptor site, its theoretical modeling is far to be trivial, as often underlined in literature[2]. Beyond the additional difficulties represented by the quantum chemical effects affecting the transfer of a light hydrogen atom (that will not be the object of this paper)[3,4], an accurate description of the Potential Energy Surface (PES) of the PT reaction requires sophisticated computational methods. Indeed, as for other properties, the "gold standard" Coupled Cluster (CC) approach should be used to obtain reliable reference for reaction and activation energies[5]. If efficient approximations, such as domain-based local pair natural orbital (DLPNO)[6] or F12[7,8], allow for the application of CC methods to large systems[9], still the associated computational effort could be high to be routinely affordable for most users and, thus, a detailed exploration of the PES could be prohibitive.

Not surprisingly, Density Functional Theory (DFT) has imposed as a reliable alternative, especially when large systems are studied[3,10-15]. Indeed, recent benchmarks indicate that the accuracy on energy barriers is comparable with that obtained by CCSD(T) methods (that is deviations lower than 5%) when using exchange-correlation functionals including global, range-separated and double hybrids (noted in the following as GH, RSH and DH, respectively)[10]. Generalized Gradient Approximations (GGAs), being largely affected by the Self-Interaction Error (SIE), significantly underestimate the barriers for PT[10,15]. Indeed, among the best functionals for PT reactions can be counted CAM-B3LYP and ωB97X-D, two RSHs containing a large amount of exact exchange (EXX, see Table 1)[10].

We have recently pointed out the *pros* and *contra* concerning the use of different exchange correlation functionals, analyzed by static approach, i.e. locating stationary points on the PES and then evaluating energy differences (reaction energies and barriers), can be translated to dynamics studies, where the PT mechanism is modelled using ab-initio molecular dynamics (AIMD) approaches[16]. Our previous analysis carried out on two small model systems, namely the malonaldehyde molecule and the formic acid dimer, indicates that the choice of the functional affects the global shape of the potential of mean force (PMF) obtained from biased molecular

dynamic trajectories, both in terms of barrier heights and form of the minimum-energy wells, in analogy to what usually found for static DFT calculations[16].

Here we want to extend this analysis by considering a more complex system, namely [2, 2'-bipyridyl]-3-3'-diol (see Figure 1), that experiences a keto-enol tautomerization (see Figure 1). During this reaction, the molecule undergoes to a double proton transfer that may occur in a concerted or stepwise fashion, if the two protons are transferred simultaneously or in two consecutive steps, respectively. Furthermore, the electronic structure, and in particular the delocalized π-electrons, experiences a significant rearrangement in going from one tautomer to the other. This molecule thus represents a much more challenging playground with respect to the simpler systems, malonaldehyde and formic acid dimer, already studied in reference 16.

In this work, the Atom Centered Density Matrix Propagation (ADMP) approach[17-19] to AIMD, coupled to an enhanced sampling algorithm[20], is used to explore the Free-Energy Surface (FES) of the reaction using several different exchange correlation functionals. The results obtained are then compared the features arising from an analysis of the PES carried out by locating the relevant stationary points and the corresponding minimum energy paths. For sake of simplicity, the latter approach will be defined in the following as *static*, juxtaposed to the term *dynamic* used for AIMD simulations.

Since the system considered in the present work is structurally more complex with respect to our previous case study, the comparison between the results obtained from the static and the dynamic approaches will allow to better exemplify the ability of the different exchange correlation functionals in reproducing reaction mechanism and in particular, related to the question concerning the synchronicity of the PT reactions and the stability of the keto-enol intermediate in [2, 2'-bipyridyl]-3-3'-diol (Figure 1)[21-23]. Indeed, this point has been explored more recently, but with contradictory results[24, 25].

2. Computational details

As first step, a preliminary static exploration of the PES was performed using the exchange-correlation functionals[26-41] reported in Table 1 in conjunction with the 6-311+G(d,p) basis set. This valence triple-ζ basis augmented with diffuse functions is chosen as trade-off between accuracy and computational effort since our aim is to consistently compare the results obtained at static and dynamic level.

Each structural optimization was carried out with very tight convergence criteria, using the C_{2h} symmetry for the di-keto and di-enol tautomers, while all the other intermediates were constrained to a C_s point group. All the optimized structures were then characterized by computing harmonic frequencies, so to characterize the nature of the extrema (minimum or transition state). All DFT calculations indicate, therefore, planar rearrangements, corresponding to an extended electronic conjugations[24].

A part for the ωB97XD and the DSD-PBEP86 models, all the other functionals do not contain any corrections for dispersion interactions. The effect of empirical potentials on H-bond energies or PT barriers is indeed low and not necessarily in the right sense[10,42]. We have, however, verified this effect, and the relative stabilities of the di-keto and di-enol tautomers, computed with the BLYP, B3LYP and CAM-B3LYP functionals vary of less than -0.1 kcal/mol (max about 1%) upon the inclusion of the D3 potential[43]. For this reason, dispersion effects will be not further discussed in the following.

Biased MD simulations were performed using the ADMP method, an extended Lagrangian method with propagation of the density matrix[17-19]. Making use of Gaussian basis functions, this approach allows for an efficient implementation of GH and RSH functionals as well as more standard GGA models. As a consequence, all functionals considered for the static study were also used for ADMP calculations, with the exception of DHs, for which the ADPM algorithm is not implemented. Additionally static data for the M11 functional are reported in SI.

Reference values were obtained via single point energy calculations carried out at the CCSD(T)-F12/cc-pVTZ-F12-CABS level of theory. This method requires a nearly-complete auxiliary basis (CABS) in addition to the orbital basis set[44]. For sake of clarity, it should be mentioned that accurate studies, carried out on smaller molecules, showed that levels of theory similar to this (CCSD(T) + triple-ζ basis set) provide reaction[45] or conformational[46] energies with an accuracy (error of 3-4%) that we consider sufficient for the aims of this paper, also in view of the large size of the investigated system and consequent favorable accuracy/cost ratio of the chosen approach. Different structures were considered for CCSD(T) calculations namely the ones optimized at MP2, M06 or B2-PLYP level. The results obtained are reported as CCSD(T)//MP2, CCSD(T)//M06 and CCSD(T)//B2-PLYP, respectively.

All static and AIMD calculations were performed using the Gaussian program[47], with the exception of the CC and MP2 calculations that were done with the ORCA program[48].

In order to perform biased MD simulations, a local version of the Gaussian program was interfaced with the PLUMED package[49], enabling to evaluate the FESs for the PT reaction using the umbrella sampling method.

The exploration of FES is obtained thanks to a harmonically biased potential, defined as:

$$V(CV) = \frac{k}{2}(CV - s_0)^2 \quad (1)$$

Where s_0 represents the collective variable at the reference structure and k is the harmonic force constant which is function of the temperature T and of the standard deviation of the collective variable σ_{CV}^2:

$$k = \frac{k_B T}{\sigma_{CV}^2} \quad (2)$$

Two collective variables have been chosen in order to better describe the PT mechanism, namely:

$$CV_1 = |R(N_3) - R(H_1)| - |R(O_5) - R(H_1)| \quad (3a)$$

$$CV_2 = |R(N_4) - R(H_2)| - |R(O_6) - R(H_2)| \quad (3b)$$

where $R(N_i)$ $R(O_i)$ and $R(H_i)$ stand for the position of atoms N_i, O_i and H_i, respectively (refer to Figure 1 for atoms labelling).

The use of these two independent collective variables allows for the construction and the analysis of the FES for both concerted and stepwise mechanisms and thus to get better insights on the reaction mechanism.

Ten configurations were collected, sampling the structures every +0.5 Bohr of the CV value along the reaction path described by the Intrinsic Reaction Coordinate (IRC). Each of these structures provides the input for the biased dynamics at constant energy carried out with an integration time step of 0.2 fs for 3 ps. Energy conservation has been verified for all the biased dynamics by linear regression of the total energy, which is around ~10^{-8} (Hartree/ps). These simulations are preceded by an equilibration run of 1.5 ps at room temperature (300K) utilizing the nuclear kinetic energy thermostat[17], implemented in the Gaussian program.

The sampling of the phase space is determined by the value of the force constant (k): large k values allow the exploration close to s_0, while small values are needed to reach regions in phase space far from the energy minima. However, energy conservation in the biased simulations is more problematic with small k-values than with large ones. For this reason, to get an optimal accuracy to efficiency ratio, different k values were chosen along the reaction path: 0.005 Hartree/Bohr^2 for

minimum-energy configurations, 0.10 Hartree/Bohr^2 for intermediate structures and 0.20 Hartree/Bohr^2 for TS.

The weighted histogram analysis method (WHAM)[50] was then used for each acquired trajectory to reconstruct the full FES at room temperature with a convergence criterion of 1 10^{-5} a.u.

Since the main aim of the paper is to compare the static and the much-more demanding dynamic computations in fair way, a computationally affordable basis set have been used. All DFT static calculations have been carried out with the 6-311+G(d,p) basis set, while, the smaller 6-31G(d,p) basis set was used for all the atoms in the ADMP calculations, except for the N, O and H atoms involved in the PT mechanism. For these latter, diffuse functions were added, leading to a modified 6-31+G(d,p) after optimization of their exponents to reproduce the PT barriers obtained with the original 6-311+G(d,p) basis set on all atoms. This combination of basis sets is hereafter defined as 6-31+G(d,p)^{AIMD}. Optimized exponents for the 6-31+G(d,p)^{AIMD} are reported in Table S1 in SI. The stationary points and the Intrinsic Reaction Coordinate profiles[51,52] were computed with 6-31+G(d,p)^{AIMD} for several xc-functionals and compared with the 6-311+G(d,p) to verify the quality of the adopted basis set in the ADMP simulations. As reported in Table S2 of the SI, the energy differences between the two basis sets for a given xc-functional are less than 0.5 kcal/mol. In other words, the modified basis set represents an acceptable balance between accuracy and computational cost savings.

3. Results and discussion

3.1 Static Proton Transfer: 1 or 2 protons at time?

As mentioned before, we will firstly analyze the results obtained using a static approach to describe the PT mechanism. Relative energies of different tautomers and TSs (Figure 1) computed with the different functionals are reported in Table 2. The reference energy is here taken as that of the highest-energy tautomer, that is the di-keto one (**1**). This choice, somehow antithetic to the usual preferences, was done to be coherent with the following ADMP simulations, carried out for convenience from the highest-energy TS structures.

Based on chemical intuition and in agreement with previous works[23] the tautomerism can proceed following two mechanisms (Figure 1), that are : i) a concerted and synchronous double proton transfer, or ii) a stepwise PT that may involves the formation of a keto-enol intermediate, (**2** in Figure 1).

Considering the resonant forms of the two stable tautomers, the di-keto one (**1**) can be formally represented by two zwitterionic resonant forms one characterized the presence of negative (positive) charges on the oxygen (nitrogen) atoms and another characterized by the presence of carbanions and positively charged nitrogens. The di-enol form (**3**), on the other hand, is restoring a full aromaticity of the cycles, resulting in a more stable formally non-zwitterionic structure.

An analysis of the electronic structure corresponding to the di-keto, keto-enol and di-enol forms performed computing the charge centroids of the Boys localized molecular orbitals is reported in Figure 2 in the case of the BLYP functional. Of note, all other functionals provide the same qualitative picture. Interestingly, the resonant form corresponding to the presence of a keto group (C=O) a carbanion and a positively charged nitrogen, seems to be the most relevant for the keto form both in the di-keto and the keto-enol intermediate (see Figure 2 and discussion below).

Qualitatively, all the considered DFT methods coherently predict the di-enol form (**3**) as the most stable, in agreement with the results obtained at the HF, MP2 and CCSD(T) level. Nonetheless, the computed relative stabilities are significantly different depending on the method selected. Considering DFT approaches, the di-enol stabilization ranges from -5.62 kcal/mol (at PBE level) to -19.68 kcal/mol (at the DSD-PBEP86 level), with many of them providing values close to the CCSD(T) estimate (that is between -13.4 and -14.6 kcal/mol).

More carefully inspecting the results reported in Table 2, a correlation between the percentage of EXX exchange present in the functional form (see Table 1) and the stabilization of the di-enol form can be noticed, the higher the EXX contribution the greater the stabilization.

The reason of the large underestimation of stabilization observed for the GGA functionals with respect to the CCSD values can be (qualitatively) ascribe to Self-Interaction Error (SIE), which predicts as smaller relative energy in the case of the charge separated zwitterionic di-keto form with respect to the corresponding di-enol one. The inclusion of EXX partially curing the SIE leads to a more realistic estimate of the two tautomer relative energies, and particularly a better estimate of the di-keto and keto-enol forms.

In order to quantitatively correlate the relative energies to the SIE, the so-called delocalization error (DE)[49] has been estimated by computing the difference between the ionization potential of a cluster of 16 He atoms located at very large interatomic distance (10 Å) and that of a single He atom as recently proposed in literature[53,54]. In absence of DE, the two ionization potentials are equal, where a large DE leads to lower potentials for the cluster, due to an over delocalization of the hole. In

Figure 3 it is plotted the energy difference between the di-keto and di-enol forms as function of the so-computed DE. A clear linear correlation between the two quantities is found, that nicely confirms the physical origin of the observed variations in relative stability.

In order to assess the accuracy of the different functionals, the deviation of the computed DFT energy differences should be assessed with respect to reference post-HF calculations. As previously mentioned, the CCSD(T) approach is recognized as the gold standard approach able to provide thermochemistry with chemical accuracy, that is an error of 1 kcal or even less[11]. However, it is very difficult, or even impossible, to optimize the geometrical structure of the two isomers (and eventually the corresponding TS) at this level of theory. Following a common practice[55], we have therefore, considered three different geometries optimized at the MP2, M06 and B2-PLYP level, three approaches providing accurate structural properties[56] but different PT mechanism in our case. The evaluation of CC energies at the MP2 structure would have been sufficient, but two striking features appear. First of all, the structure of the di-enol form, in contrast with the DFT results, is not planar, due to spurious effects on the electronic correlation well documented in literature[57]. This drawback could also explain the high stability computed for the di-enol form, that is found to be very close to that provided by the HF method (-25.7 vs. 26.5 kcal/mol). The CCSD(T) on the molecular structures obtained with both M06 and B2PLYP functionals are, instead, similar (about -14.6 kcal/mol), even if these functionals suggests two different reaction mechanisms (see infra). We prefer, therefore, to select the CCSD(T) value computed using these structures as reference to evaluate the accuracy of the DFT approaches.

On this basis, the analysis of the energies reported in Table 2 suggests that local GGA functionals, that is BLYP, PBE and M06-L, as well as two GHs with a relatively low percentage of EXX (B3LYP and PBE0) underestimate the stability of the di-enol tautomer with respect to the di-keto one. In contrast, DSD-PBEP86 provides a too large stabilization (-19.7 kcal/mol). Values in reasonable agreement (± 2 kcal/mol) with the CCSD(T) reference are obtained with all the other functionals, even if the dispersion of the results is still relative large, from -12.0 kcal/mol computed at M06 level to -16.4 kcal/mol for M06-2X. The strong dependency of these energies upon the EXX contribution is also evident, large EXX values in the functional providing larger stabilities, as already discussed.

Next, the PT mechanism was studied at the different level of theory to identify which one, between a concerted or a stepwise mechanism, was predicted to be relevant by the different functionals considered.

The concerted mechanism is characterized by a stationary point corresponding to a simultaneous double PT (equivalent to TS_D in Figure 1), structurally characterized by the same point group symmetry of the two minima (C_{2h}). This structures, has indeed been localized considering only four functionals, namely: B2-PLYP, ωB97XD, B3LYP and BLYP. For the first three, the TS is about 35 kcal/mol higher in energy that the di-keto tautomer (**1**), while the last functional, BLYP, provides a lower value (about 21 kcal/mol). All these four TSs are characterized by the presence of two imaginary frequencies, corresponding to the symmetric and antisymmetric stretching of the N-H bond, with displacement of the protons toward the acceptor O atom (see Figure S1 and Table S3 in SI). In other words, these functionals predict a second-order saddle point for the concerted PT, but very high in energy. Based on these results, this mechanism has been therefore discharged for all the DFT methods, in favor of a stepwise mechanism. Ideally, two TSs are excepted corresponding to the sequential transfer of the first and, then, of the second proton. As we will see, this is not always the case.

The energy corresponding to the relevant intermediates and TSs are reported in Table 2 together with those of the stable di-keto and di-enol tautomers. Most of the functionals agree in locating a single TS between the two energy minima, the exception being BLYP, M06-L and M06, for which a stable keto-enol intermediate and two TSs can be localized along the reaction path.

Let us start the discussion from the results obtained for majority of the functionals. In this case a single TS (labelled as TS_1 in Table 2 and Figure 1) can be located. Depending on the functionals the energy barrier from the di-keto ranges from 0.04 (M06-2X) to 1.7 (B2-PLYP) kcal/mol. The CCSD(T) reference value is around 0.6-0.7 kcal/mol (see also below) and only 4 functionals, namely M11, CAM-B3LYP, PBE0 and PBE give values in reasonable agreement with this reference (see Table 2 and SI). For the others the barrier is computed to be significantly higher, between + 40% and 140% of the refence value (corresponding to an overestimation of the barrier of 1 to 1.7 kcal/mol). This behavior may appear surprising, in view of previous benchmarks on PT systems[2,10,11,15], and it points out the subtle electronic effects that are at play in [2,2'-bipyridyl]-3-3'-diol and its substantially difference with respect to model systems. Notably, the acceptable barrier obtained at the PBE level (0.46 kcal/mol) could be attributed to an error compensation,

since it is well known that this functional significantly underestimate energy barrier for PT[11,15]. Indeed, in the present case the anomalous overstabilization of the di-keto tautomer already pointed out and due to SIE is probably at the origin of the relatively good estimate of the barrier.

The inclusion of EXX in PBE0 partially corrects the SIE error and the overstabilization of the di-keto form, significantly improving the predicted relative stabilities of the two tautomers, but it leads to a slight deterioration of the barrier value. Both PBE and PBE0 are also the functionals predicting a relative small curvature at the saddle point, with an associated imaginary frequency (ν_1, Table 2) below 800i cm^{-1}, while all other functionals suggest values close to 1000 cm^{-1} or higher, with the exception of M06-2X and M11 which are also predicting a very flat PES (ν_1 of 389icm-1 and 754i cm-1, respectively, Table 2 and SI). Interestingly, the normal mode associated to the imaginary frequency for all functionals corresponds to the transfer of a single proton.

From a structural point of view for all the functionals showing a single barrier, one of the NH bond increases in going from the di-keto to the TS, typically from 1.06 to 1.20 Å, while the corresponding N-O distance is reduced, in average from 2.54 to 2.45 Å. The large flexibility of the structure helps in reducing the energy barriers for the first PT. From the TS, the di-enol structural parameters, with equal OH and NO distances, are then easily recovered.

These results suggest that a small energy is required to move the first proton and then activate a second barrierless PT. In other term, the reaction is not fully concerted since the two protons are not transferred simultaneously neither the protons are sequentially transferred so that a first and second PT can be clearly distinguished. We could speak, instead, of an *asynchronous* double PT, where the movement of the second proton (barrierless) is activated by the transfer of the first.

For 3 functionals, BLYP, M06-L and M06, however, the reaction is stepwise since two distinct TSs have been identified and characterized by relatively high imaginary frequencies (between 980i and 1400i cm^{-1}, approximately). In this case, the transfer of the protons is sequential, with two well-distinct movements, as can be easily view by looking at the atomic displacements along the two imaginary modes (see data reported in SI). In these 3 cases the PES between the di-keto and the keto-enol form is (very) flat, the energy of the keto-enol intermediate being -0.94, -1.47 and – 3.52 kcal/mol for BLYP, M06-L and M06, respectively. The second barrier in any case significantly smaller that the first one (Table 2). At the same time, the NH lengths involving the transferred proton increases from about 1.05/1.07 Å to about 1.66/1.70 Å, while the NO distance is almost constant (about 2.57-2.60 Å). Then the di-enol form is reached through a second TS, slightly higher

in energy with respect to the keto-enol form. The small height of this second barrier (between 0.01 kcal/mol for BLYP and 0.84 kcal/mol for M06-L) could suggest that, at least for the BLYP case, the limit of the numerical precision of our calculation is reached. However, the associated imaginary frequencies (between 1000i and 1400i cm^{-1}) and the displacement vectors (see SI) allow to discharge this hypothesis and confirm the existence of an intermediate and of a second TS.

In order to get further insights allowing to understand the peculiar behavior obtained by the BLYP, M06-L and M06 functionals, we decided to characterize the electronic structure corresponding to all extrema of the PES by analyzing the charge centroids of the Boys localized molecular orbitals[58]. This type of analysis is reported, in Figure 2, for the BLYP functional. First of all, it is interesting to note that all forms containing a keto group (di-keto, and keto-enol) are characterized by the presence of a carbanion in the same ring of the keto moiety. As a consequence a doubly zwitterionic form and the one corresponding to a carbanion on the keto containing ring and a positively charged nitrogen on the enol ring are the most relevant resonant forms predicted by the Boys analysis for the di-keto and the keto-enol forms, respectively. Interesting the intermediate seems to be characterized by the presence of one fully aromatic ring (the ring carrying the enol group) while full aromaticity of the ring is restored for the most stable di-enol form. Both the first (TS_1) and the second (TS_2) transition states are electronically very close to the products that are the keto-enol and the di-enol forms respectively. Both TSs actually show already a full recover of the aromaticity in the enol containing ring(s) and that before the full occurring of the proton transfer. However, while the relative stability of the different forms well correlates with the DE observed for the three functionals it is not possible to directly connect the corresponding reaction barriers to the DE, pointing out that other non-easily-identifiable effects must also contribute.

Finally, the M06-2X functional has an atypical behavior, with a very low barrier for a single PT (0.04 kcal/mol) associated to a low imaginary frequency (389i cm-1), whose displacements concerns both protons. These values indicate a nearly barrierless PT. Furthermore, the M06-2X is the only functional giving an almost C_{2h} high-symmetric structure for the TS. For instance, the two OH distances for the two transferred proton are very close, being 1.42 and 1.52 Å. Previous calculations, carried out using the smaller 6-31G(d,p) basis set, report a stable keto-enol form, -6.27 kcal/mol more stable than di-keto, in clear contrast with the present results and no TSs were characterized in the literature[24]. This effect could be easily ascribed to the small basis set that,

lacking the necessary diffuse functions for an accurate evaluation of PT energies lead to a stabilization of the keto-enol form.

As for the relative stabilities of the di-enol form, the energy of the reactive intermediates has been assessed by carrying out CCSD(T) calculations on MP2, M06 and B2-PLYP geometries. As for the energy minima, the estimation of the TS_1 energy is very close being between 0.60 and 0.70 kcal/mol (see Table 2). Interesting, when using the M06 geometries, corresponding to a stepwise mechanism, the CCSD(T) total energies computed for the keto-enol form and the TS_2 are higher than that for the TS_1 point (see SI, Table S4). In absence of a full CCSD(T) geometry optimization, these data strongly suggest that an asynchronous PT mechanism is also probable for the CCSD(T) method.

Finally, Intrinsic Reaction Coordinates (IRC) calculations have been carried out to confirm that the localized TSs connect the di-keto with the di-enol form. Selected IRC profile are reported in Figure 4, while all others are collected in the SI. All the functionals showing a single TS present a plateau in going from the TS to the di-keto form, whose extension (slightly) varies as a function of the functional considered. For instance, B3LYP and ωB97XD have the longest plateau, reaching a value of the reaction coordinate of about 3.0 Å $amu^{1/2}$. Notably the CAM-B3LYP, B2-PLYP and B3LYP profiles are practically parallel, even if slightly shifted, thus well evidencing their common features. A second TS is, as discussed, not localized with these functionals, but their IRC profiles present a clear inflection followed by a sudden drop of the energy before reaching the most stable di-keto isomer. This sudden drop well underlines a transfer of the second proton activated by the movement of the first. These features are less evident in the M06-2X profile, where the movement of the second proton take place shortly (in the reaction coordinate space) after the first PT.

In summary, the static study of the PT mechanism in [2,2'-bipyridyl]-3-3'-diol, carried out by characterizing the stationary points (minima and TSs) well evidence its dependence on the functional choice. Most of the selected functionals provide an asynchronous mechanism where the first PT activates the second one. On the other hand, few functionals, namely BLYP, M06-L and M06, indicates a step-wise mechanism, where protons are transferred sequentially and enabling to identify a stable keto-enol intermediate.

3.2 Dynamic view of Proton Transfer: the Free-energy profiles

At this point it is interesting to confirm if the features observed on the PES (static calculations) are preserved in the FES (dynamic calculations). It is worth to underline that, as already done[16] , the comparison between PESs and FESs is only qualitative since they are different by their definition and since the latter (FESs) are here computed using the smaller -optimized- basis set 6-31+G(d,p)^{AIMD} (see computational details and SI for its definition).

In Figure 5 are reported the 2D maps of the FES computed using two GGA functionals, namely M06-L and PBE. The surface generated with the M06-L functional (Figure 5 left) is characterized by the presence of three minima, corresponding to the di-keto, keto-enol and di-enol forms. These minima are then connected by two transition states representing the transfer of the two protons associated with each of the two collective variables. The energy color gradient shows that the kinetic determining step is the first, as predicted by the static calculations. The FES map indicates that the energy variations along one of the CVs, e.g. CV1, are accompanied by (relatively) small fluctuations of the other coordinate, e.g. CV2 (ΔCV_2 of about 0.5 Å for $\Delta\Delta F$ of about 0.1 kcal/mol). This feature shows that the two CVs are practically uncoupled and support the description of the reaction mechanism as stepwise: a first proton is transferred, corresponding to a variation of about 2.5 Å of the CV_1, followed by the second proton movement, with similar amplitude ($\Delta CV_{1,2} \approx 2.5$ Å).

This is not the case for PBE, where the topology of the FES is significantly different. Indeed, the reaction path streams in large energy valleys (Figure 5, right) characterized by a first deep energy minimum for the di-enol form and a second, higher in energy, for the di-keto tautomer. Among the two a TS can be barely localized. The amplitude of the CVs is smaller than for M06-L ($\Delta CV_{1,2} \approx$ 2.0 Å), but the two CVs are partially coupled especially close to the di-keto form that lies in large shallow region of the FES. In this sense, the transfer of the second proton is activated well before the TS.

The inclusion of EXX into the functional somehow alter the topology of the FESs, as it could be expected. In Figure 6 are reported the map energies for three GHs, B3LYP, M06 and M06-2X, and one RSH, ωB97XD. The results for the other functionals are collected in the SI.

M06-2X, an hybrid functional containing 54% of EXX, provides a FES with features similar to what observed with PBE (Fig. 5). Indeed, a deep minimum for the di-enol form can be easily identified, whereas the di-enol species, higher energy, can be reached through a single TS. Also in this case, the two CVs are significantly coupled and the FES is markedly shallow in correspondence

of the two energy minima. This energy landscape significantly favors the concurrent movements of the protons. Notably, the two CVs span over a larger interval ($\Delta CV_{1,2} \approx 3.0$ Å).

At a first sight, B3LYP and M06, the two other GHs, provide very similar topologies for the surfaces, albeit the relative energies of the stationary points are, as expected, different. In both cases, the two CVs are almost uncoupled and they range over an interval longer than in the previous cases ($\Delta CV_{1,2} \approx 3.5$ Å). A deeper analysis however shows that a shallow minimum, around ΔCV_1 = -1.0 Å and ΔCV_2 = 1.5 Å, is present for M06, as well two TSs. Despite the low values of the relative energies (see infra), we are in presence of a stepwise mechanism for the PT. It should also remarked that in both cases the FES is shallow before the TS, so that, also in this case, the second PT is facilitated by the first. However, a larger shallow minimum for the di-keto form is observed for the B3LYP functional than for M06.

Finally, the ωB97XD RSH has an intermediate behavior, providing a FES where only two energy minima can be clearly identified, connected by a single TS, but the reaction channel for the movement of the second proton is quite large, the FES significantly widening ($|\Delta CV_1| \approx 1.0$ Å) before and after the first proton has passed through the TS.

In order to more easily evidence the differences between the different functionals in Figure 7 are reported the free-energy profiles evaluated as minimum energy paths on the computed FESs, having as reference-energy that of the first TS. A subsequent interpolation with a fifth-degree polynomial have been then used to smooth the profiles. These profiles well evidence the different features of the FES already discussed. For instance the shallow minimum corresponding to the intermediate keto-enol form is clearly evident for the profiles obtained with the M06-L and M06 functionals. The other curves do not show any clear minimum (and associated TS_2) even if they are quite flat at the corresponding values of the associated CVs. The length of the plateau and the following slope in energy leading to the di-enol tautomer change with the functional, the PBE providing the smoothest and M06-2X the stiffest profiles. Interestingly, the M06-2X functional give a minimum at values of the CVs coordinate close to that of the other functionals, while its IRC profile was the shortest one. From these profiles it is also possible to give an estimate of the relative free energies of the stationary points, as reported in Table 3.

4. Comments and conclusions

The coupling of the exploration of the PES carried out by localizing stationary points (TS and minima) and associated IRC path with the study of the FES conducted by ab-initio molecular dynamics, both performed making use of different Density Functional Approximations, allows to acquire detailed information on the PT mechanism in a complex molecule such as [2,2'-bipyridyl]-3-3'-diol. Of the two possible mechanisms, namely a concerted transfer of the two protons and a stepwise movement of a protons after the other, the first one is clearly discharged. Indeed, the corresponding TS state, localized for some selected functionals, and corresponding to a second order saddle point is lying at very high energy.

The reaction features associated with the second mechanism, stepwise, then depends on the selected functionals. Three among the functionals considered in the present study, namely BLYP, M06-L and M06, suggest a clear stepwise mechanism, where the protons are transferred sequentially. This description arises from the localization, on both PES and FES, of a stable keto-enol form and of two distinct TSs along the reaction path.

In contrast all other functionals provide a slightly different description where the movement of the second proton takes place after the first one has reached the TS. This reaction can be described as an asynchronous activated PT, where the movement of the first proton induces a second barrierless PT, thus resulting in the transfer of the two protons, with only the first occurring via a well-defined TS. The analysis of the associated FES shows that the coupling between the two CVs describing the PT increases close to the TS, thus well evidencing the enhancement effect of the first PT on the second. B3LYP, BH&HLYP, PBE0, CAM-B3LYP, PBE, ωB97XD all provide this same mechanistic picture.

Only M06-2X has a further different behavior, where the localized TS corresponds to the movement in majority of a first proton but has small component on the second proton. This feature, together with similar bond lengths for the H atoms involved in the transfer, lead to a description of the mechanism closing resembling to a fully concerted PT, where the two protons move at the same time.

From this context appears that the differences observed between the functionals go well beyond those concerning the computed energies values (and their agreement with the reference values when available). Indeed, different functionals lead to different mechanisms thus affecting the chemical interpretation of the process under investigation (here PT).

Thanks to the comparison with reference post-HF data obtained for the static approach, it has been possible to show how discrepancies between the functionals and from the reference data may be correlated to the different degrees of SIE that it is affecting the functionals. Indeed, in this specific case, the small energy barriers and the overall relative stability of the different tautomers are strongly affected by the ability of the functionals to describe with the same accuracy localized, zwitterionic and delocalized electronic structures. Functionals that are more largely affected by SIE, tends to over stabilize delocalized electronic structures and thus provide a picture somehow even qualitatively different to that of provided by all others.

References

1) Hammes-Schiffer, S. Virtual Issue on Proton Transfer. *J. Phys. Chem. B* **2021**, *125*, 3725.

2) Nachimuthu, S, Gao, J., Truhlar, D.G. *Chem. Phys.* **2012**, *400*, 8.

3) Pu, J., Gao, J., Truhlar, D.G., *Chem. Rev.* **2006**, *106*, 3140.

4) Peters, K.S. *Acc. Chem. Res.* **2009**, *42*, 89.

5) Karton, A. *J. Phys. Chem. A* **2019**, *123*, 6720.

6) Riplinger, C.; Pinski, P.; Becker, U.; Valeev, E. F.; Neese, F. *J. Chem. Phys*. **2016**, *144*, 024109.

7) Kong, L.; Bischoff, F. A.; Valeev, E. F. *Chem. Rev.* **2012**, *112*, 75.

8) Hättig, C.; Klopper, W.; Köhn, A.; Tew, D. P. *Chem. Rev*. **2012**, *112*, 4.

9) Ni, Z.; Guo, Y.; Neese, F.; Li, W.; Li, S. *J. Chem. Theory Comput*. **2021**, *17*, 756.

10) Mangiatordi, G. F.; Brémond, E.; Adamo, C. *J. Chem. Theory. Comput*. **2012**, *8*, 3082.

11) Karton, A.; O'Reilly, R. J.; Radom, L. *J. Phys. Chem. A* **2012**, *116*, 4211.

12) Medina, F. E.; Neves, R. P. P.; Ramos, M. J.; Fernandes, P. A. *ACS Cat.* **2018**, *8*, 10267

13) Stecher, T. Reuter, K., Oberhofer, H. *Phys. Rev. Lett.* **2016**, *117*, 276001.

14) Barone, V., Adamo, C. *J. Chem. Phys.* **1996**, *105*, 11007.

15) Seyedraoufi, S.; Berland, K *J. Chem. Phys.* **2022**, *156*, 244106.

16) Brémond, É.; Savarese, M.; Rega, N.; Ciofini, I.; Adamo, C. *J. Chem. Theory Comput*. **2022**, *18*, 1501.

17) Schlegel, H. B.; Millam, J. M.; Iyengar, S. S.; Voth, G. A.; Daniels, A. D.; Scuseria, G. E.; Frisch, M. J. *J. Chem. Phys.* **2001**, *114*, 9758.

18) Iyengar, S. S.; Schlegel, H. B.; Millam, J. M.; A. Voth, G.; Scuseria, G. E.; Frisch, M. J. *J. Chem. Phys.* **2001**, *115*, 10291.

19) Schlegel, H. B.; Iyengar, S. S.; Li, X.; Millam, J. M.; Voth, G. A.; Scuseria, G. E.; Frisch, M. J. *J. Chem. Phys.* **2002**, *117*, 8694.

20) Branduardi, D.; Vivo, M. D.; Rega, N.; Barone, V.; Cavalli, A. *J. Chem. Theory. Comput*. **2011**, *7*, 539.

21) Barone, V.; Palma, A.; Sanna, N. *Chem. Physics Lett.* **2003**, *381*, 451.

22) Sobolewski, A. L.; Adamowicz, L. *Chem. Physics Lett.* **1996**, *252*, 33.

23) Barone, V.; Adamo, C. *Chem. Physics Lett* **1995**, *241*, 1.

24) Chaihan, K.; Kungwan, N. *New J. Chem.* **2020**, *44*, 8018.

25) Su, S.; Fang, H. *Mol. Phys*. **2020**, *118*, e1730990.

26) Becke, A. D. *Phys. Rev. A* **1988**, *38*, 3098.

27) Lee, C.; Yang, W.; Parr, R. G.. *Phys. Rev. B* **1988**, *37*, 785.

28) Perdew, J. P.; Burke, K.; Ernzerhof, M. *Phys. Rev. Lett.* **1996**, *77*, 3865.

29) Zhao, Y.; Truhlar, D. G. *J. Chem. Phys* **2006**, *125*, 194101.

30) Stephens, P. J.; Devlin, F. J.; Chabalowski, C. F.; Frisch, M. J. *J. Phys. Chem.* **1994**, *98*, 11623.

31) Becke, A. *J. Chem. Phys.* **1993**, *98*, 5648.

32) Adamo, C.; Barone, V. *J. Chem. Phys.* **1999**, *110*, 6158.

33) Ernzerhof, M.; Scuseria, G. E. *J. Chem. Phys.* **1999**, *110*, 5029.

34) Zhao, Y.; Truhlar, D. G. *Theor. Chem. Acc.* **2008**, *120*, 215.

35) Becke, A. D. *J. Chem. Phys.* **1993**, *98*, 1372.

36) Zhao, Y.; Truhlar, D. G. *J. Phys. Chem. A* **2006**, *110*, 13126.

37) Chai, J.D., Head-Gordon, M. *Phys. Chem. Chem. Phys.*, **2008**, *10*, 6615.

38) Yanai, T.; Tew, D. P.; Handy, N. C. *Chem. Phys. Lett.* **2004**, *393*, 51.

39) Peverati, R.; Truhlar, D. G. *J. Phys. Chem. Lett.* **2011**, *2*, 2810.

40) Kozuch, S.; Martin, J. M.. *Phys. Chem. Chem. Phys.* **2011**, *13*, 20104.

41) Grimme, S. *J. Chem. Phys.* **2006**, *124*, 034108.

42) A. D. Boese, *ChemPhysChem*, **2015**, *16*, 978

43) S. Grimme, J. Antony, S. Ehrlich, H. Krieg, *J. Chem. Phys*., **2010**, *132*, 154104

44) Adler, T. B.; Knizia, G.; Werner, H.-J. *J. Chem. Phys.* **2007**, *127*, 221106.

45) Martínez González, M.; Xavier, F. G. D.; Li, J.; Montero-Cabrera, L. A.; Garcia De La Vega, J. M.; Varandas, A. J. C., *J. Phys. Chem. A*, **2020**, *124*, 126.

46) Varandas, A. J. C. *Phys. Chem. Chem. Phys.* **2021**, *23*, 9571.

47) Frisch, M. J.; Trucks, G. W.; Schlegel, H. B.; Scuseria, G. E.; Robb, M. A.; Cheeseman, J. R.; Scalmani, G.; Barone, V.; Mennucci, B.; Petersson, G. A.; Nakatsuji, H.; Caricato, M.; Li, X.; Hratchian, H. P.; Izmaylov, A. F.; Bloino, J.; Zheng, G.; Sonnenberg, J. L.; Hada, M.; Ehara, M.; Toyota, K.; Fukuda, R.; Hasegawa, J.; Ishida, M.; Nakajima, T.; Honda, Y.; Kitao, O.; Nakai, H.; Vreven, T.; Montgomery, J. A., Jr.; Peralta, J. E.; Ogliaro, F.; Bearpark, M.; Heyd, J. J.; Brothers, E.; Kudin, K. N.; Staroverov, V. N.; Kobayashi, R.; Normand, J.; Raghavachari, K.; Rendell, A.; Burant, J. C.; Iyengar, S. S.; Tomasi, J.; Cossi, M.; Rega, N.; Millam, J. M.; Klene, M.;Knox, J. E.; Cross, J. B.; Bakken, V.; Adamo, C.; Jaramillo, J.; Gomperts, R.; Stratmann, R. E.; Yazyev, O.; Austin, A. J.; Cammi, R.; Pomelli, C.; Ochterski, J. W.; Martin, R. L.; Morokuma, K.; Zakrzewski,

V. G.; Voth, G. A.; Salvador, P.; Dannenberg, J. J.; Dapprich, S.; Daniels, A. D.; Farkas, N.; Foresman, J. B.; Ortiz, J. V.; Cioslowski, J.; Fox, D. J. *Gaussian 09 Revision A.02*. ; Gaussian Inc. Wallingford CT, 2001.

48) Neese, F.; Wennmohs, F.; Becker, U.; Riplinger, C. J. *Chem. Phys.* **2020**, *152*, 224108.

49) Bonomi, M.; Branduardi, D.; Bussi, G.; Camilloni, C.; Provasi, D.; Raiteri, P.; Donadio, D.; Marinelli, F.; Pietrucci, F.; Broglia, R. A.; Parrinello, M. *Comp. Phys. Comm*. **2009**, *180*, 1961.

50) Grossfield, A. *WHAM: the weighted histogram analysis method, version 2.0. 9.* Available at membrane.urmc.rochester.edu/content/wham. Accessed November 2022

51) Fukui, K. *Acc. Chem. Res.*, **1981**, *14*, 363.

52) Hratchian, H.P.; Schlegel, H. B. in *Theory and Applications of Computational Chemistry: The First 40 Years*, Dykstra, C. E.; Frenking, G.; Kim, K.S.; Scuseria G.E., Eds. Elsevier, Amsterdam, Netherland, 2005; pp. 195-249.

53) Zhang, Y.; Yang, W. *J. Chem. Phys.* **1998**, *109*, 2604.

54) Bao, J. L.; Wang, Y.; He, X.; Gagliardi, L.; Truhlar, D. G. *J. Phys. Chem*. Lett. **2017**, *8*, 5616.

55) L. P. Viegas, A. J. C. Varandas, J. Comput. Chem., **2014**, *35*, 507.

56) Brémond, É.; Savarese, M.; Su, N. Q.; Pérez-Jiménez, Á. J.; Xu, X.; Sancho-García, J. C.; Adamo, C. *J. Chem. Theory Comput*. **2016**, *12*, 459.

57) Moran, D.; Simmonett, A. C.; Leach, F. E.; Allen, W. D.; Schleyer, P. v. R.; Schaefer, H. F. *J. Am. Chem. Soc.* **2006**, *128*, 9342.

58) Boys, S. F. *Rev. Mod. Phys.* **1960**, *32*, 296.

Table I. List of the exchange-correlation functionals considered in this work, ranked according to the casted percentage of exact-like exchange (EXX) and second-order perturbation (PT2) correlation.

Functional	%EXX[a]	%PT2	reference
GGA			
BLYP	0	0	26,27
PBE	0	0	28
M06-L	0	0	29
Global Hybrids			
B3LYP	20	0	30, 31
PBE0	25	0	32,33
M06	27	0	34
BH&HLYP	50	0	35
M06-2X	54	0	36
Range-Separated Hybrids			
ωB97XD	22/100	0	37
CAM-B3LYP	19/65	0	38
M11	42.8/100	0	39
Double Hybrids			
DSD-PBEP86	69	22/52[b]	40
B2-PLYP	53	27	41

a) min/max for range separated hybrids, b) same/opposite contribution

Table 2. Energies (kcal/mol) relative to the di-keto tautomer (**1**, Figure 1) for the proton transfer in [2,2'-bipyridyl]-3-3'-diol. The and imaginary frequencies (ν_i, cm^{-1}) computed at the transition states are also reported. All the calculations have been carried out with the 6-311+G(d.p) basis set.

	TS_1	keto-enol (**2**)	TS_2	di-enol (**2**)	ν_1	ν_2
HF	2.23	-11.05	-10.25	-26.54	1356*i*	1014*i*
MP2	3.00			-25.67	788*i*	
CCSD(T)//MP2	0.72			-13.42		
CCSD(T)//M06	0.57			-14.62		
CCSD(T)//B2-PLYP	0.60			-14.62		
BLYP	1.44	-0.94	-0.93	-5.64	978*i*	1018*i*
PBE	0.46			-5.62	744*i*	
M06-L	2.63	-1.47	-0.63	-7.78	1401*i*	1408*i*
B3LYP	1.26			-9.69	1038*i*	
PBE0	0.40			-10.50	788*i*	
M06	1.65	-3.52	-3.24	-11.99	1496*i*	-1018*i*
BH&HLYP	1.32			-15.92	1139*i*	
M06-2X	0.04			-16.39	389*i*	
ωB97XD	0.97			-12.74	995*i*	
CAM-B3LYP	0.59			-13.07	905*i*	
M11	0.34			-12.54	754*i*	
DSD-PBEP86	1.47			-19.68	969*i*	
B2-PLYP	1.65			-16.61	1021*i*	

Table 3. Free energies (kcal/mol) relative to the di-keto tautomer (see Figure 1) for proton transfer in [2,2'-bipyridyl]-3-3'-diol. The values have been estimated from the minimum energy profiles obtained from the free-energy surfaces calculations.

	TS_1	keto-eno	TS_2	di-enol
PBE	0.60			-4.97
M06-L	2.05	-0.05	-0.22	-5.46
B3LYP	0.47			-9.25
PBE0	0.02			-8.97
M06	0.68	-1.37	-1.27	-6.77
BH&HLYP	0.60			-14.34
M06-2X	0.33			-14.80
ωB97XD	0.64			-10.98
CAM-B3LYP	1.13			-11.43

Figure captions

Figure 1 Schematic draw of species involved in single and double proton transfer in [2,2'-bipyridyl]-3-3'-diol. For the di-enol tautomer the numbering of the atoms used for the definition of the collective variables is also reported .

Figure 2 Centroids (in purple) of the Boys localized molecular orbitals computed at the BLYP level of theory for the optimized di-keto, TS_1 keto-enol, TS_2 and di-enol tautomer. .

Figure 3. Relative stabilities of the di-keto and di-enol tautomers as function of the delocalization error.

Figure 4 Intrinsic Reaction Coordinate profiles for the proton transfer reaction in [2,2'-bipyridyl]-3-3'-diol computed using selected functionals. Refer to text for level of theory.

Figure 5. Plot of the Free Energy Surface (in kcal/mol) along the two collective variables (CV, Å) computed with the M06-L and PBE functionals.

Figure 6. Plot of the Free Energy Surface (in kcal/mol) along the two collective variables (CV, Å) computed with the M06-2X, B3LYP, ωB97XD functionals.

Figure 7. Minimum free energy path (kcal/mol) for the proton transfer reaction in [2,2'-bipyridyl]-3-3'-diol, computed using selected functionals. The profile were interpolated using a fifth order polynomial. ($E = \sum_{j=0}^{k} |p(x_j) - y_j|^2$), where x_j is as a linear combination of the two collective variables.

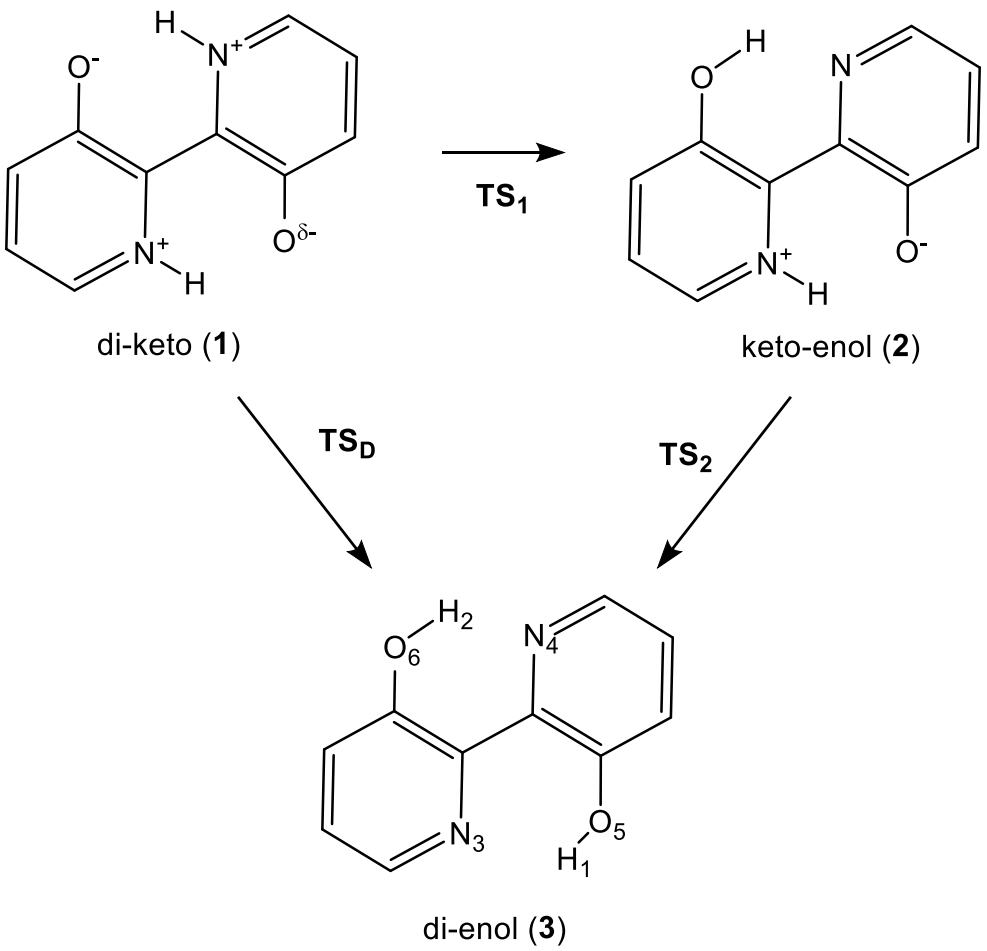

Figure 1

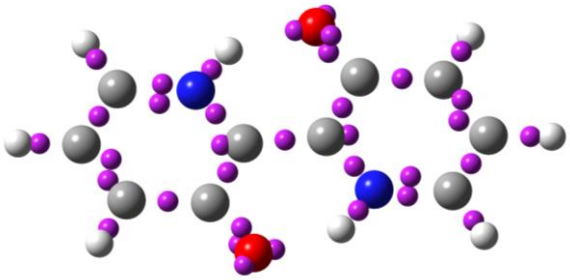

di-keto (**1**)

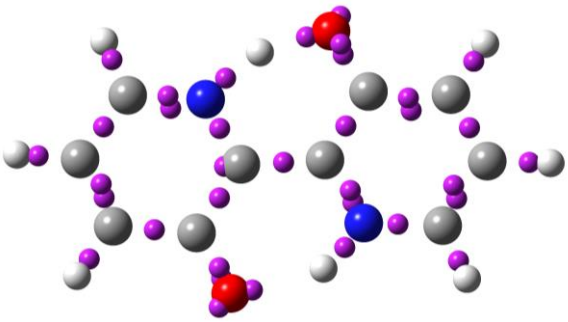

TS_1

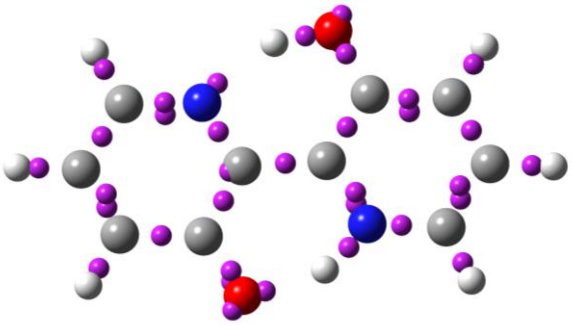

keto enol (**2)**

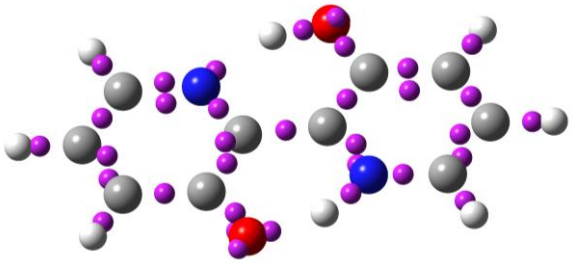

TS_2

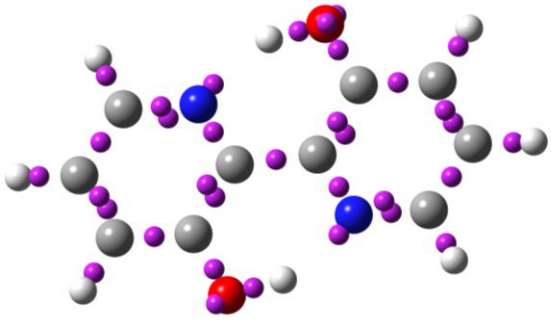

di-enol (**3**)

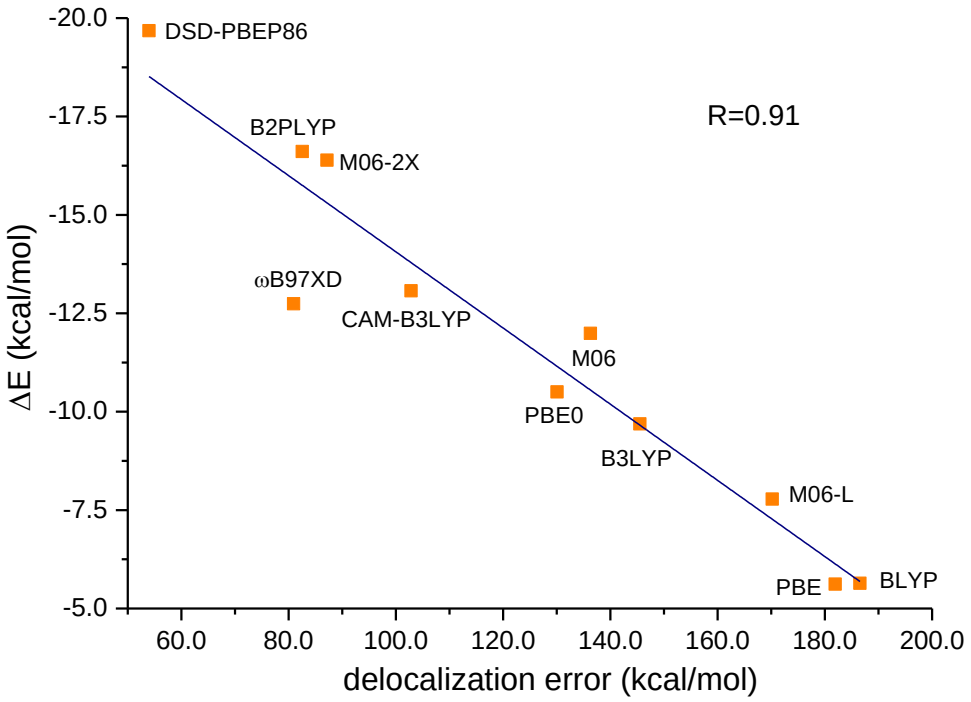
-20.0
-17.5
-15.0
-12.5
-10.0
-7.5
-5.0
ΔE (kcal/mol)
60.0
80.0
100.0
120.0
140.0
160.0
180.0
200.0
delocalization error (kcal/mol)
DSD-PBEP86
B2PLYP
M06-2X
ωB97XD
CAM-B3LYP
M06
PBE0
B3LYP
M06-L
PBE
BLYP
R=0.91

Figure 3

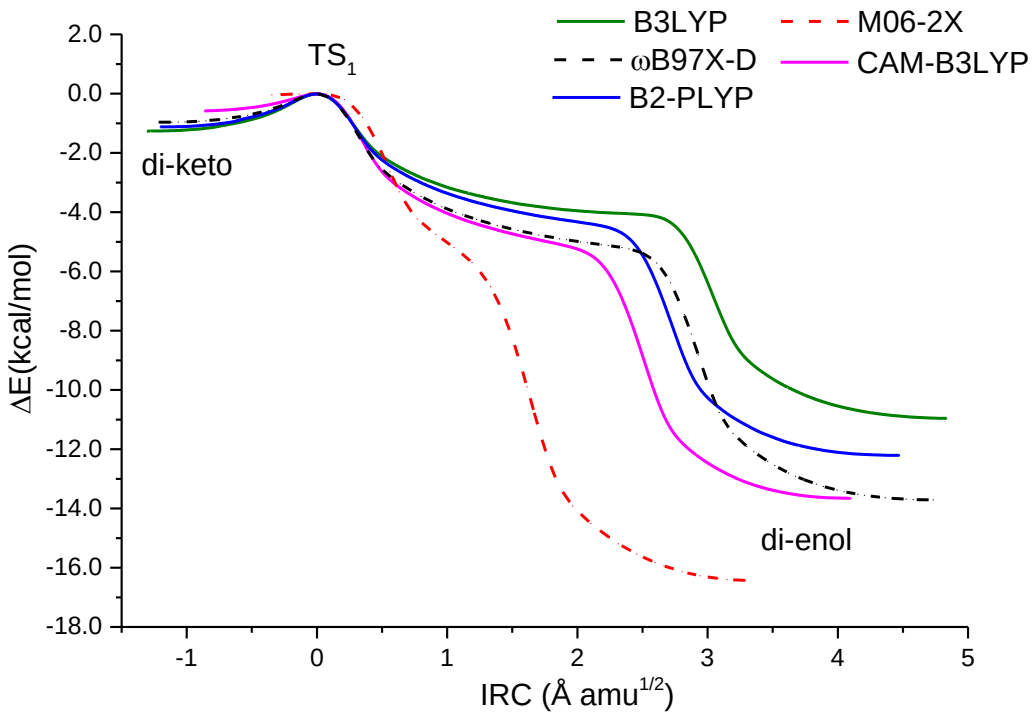
B3LYP
M06-2X
ωB97X-D
CAM-B3LYP
B2-PLYP
TS1
di-keto
di-enol
ΔE(kcal/mol)
IRC (Å amu1/2)
2.0
0.0
-2.0
-4.0
-6.0
-8.0
-10.0
-12.0
-14.0
-16.0
-18.0
-1
0
1
2
3
4
5

Figure 4

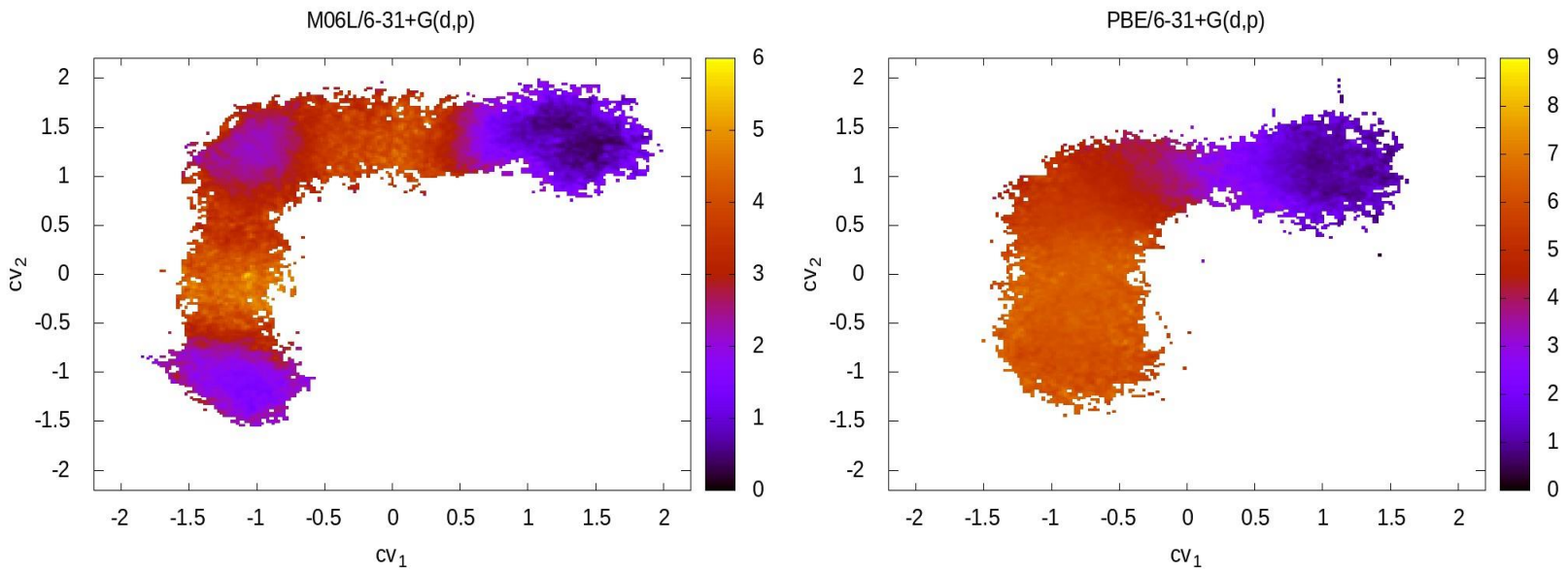

Figure 5

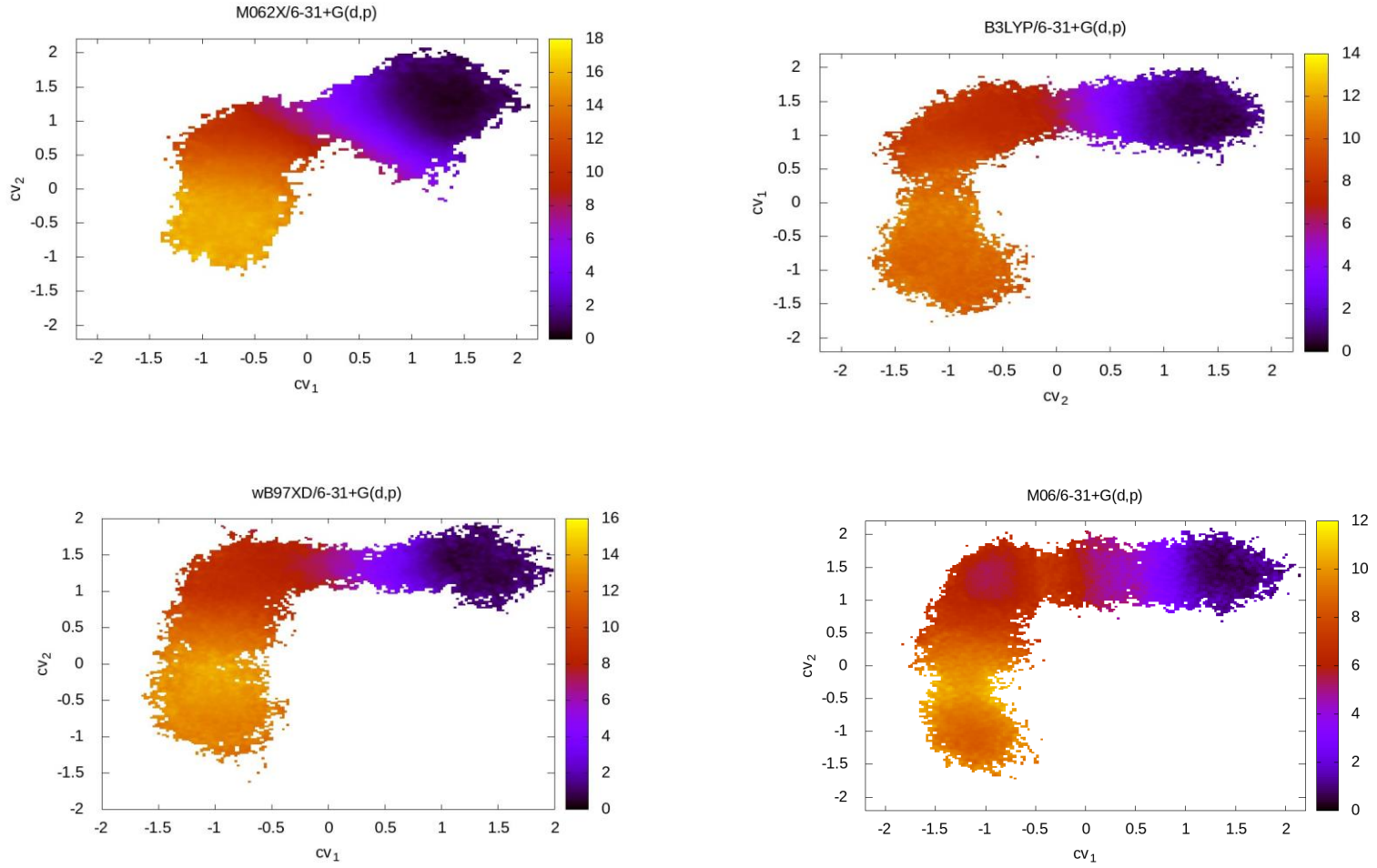
M062X/6-31+G(d,p)
cv1
cv2
B3LYP/6-31+G(d,p)
cv2
cv1
wB97XD/6-31+G(d,p)
cv1
cv2
M06/6-31+G(d,p)
cv1
cv2

Figure 6

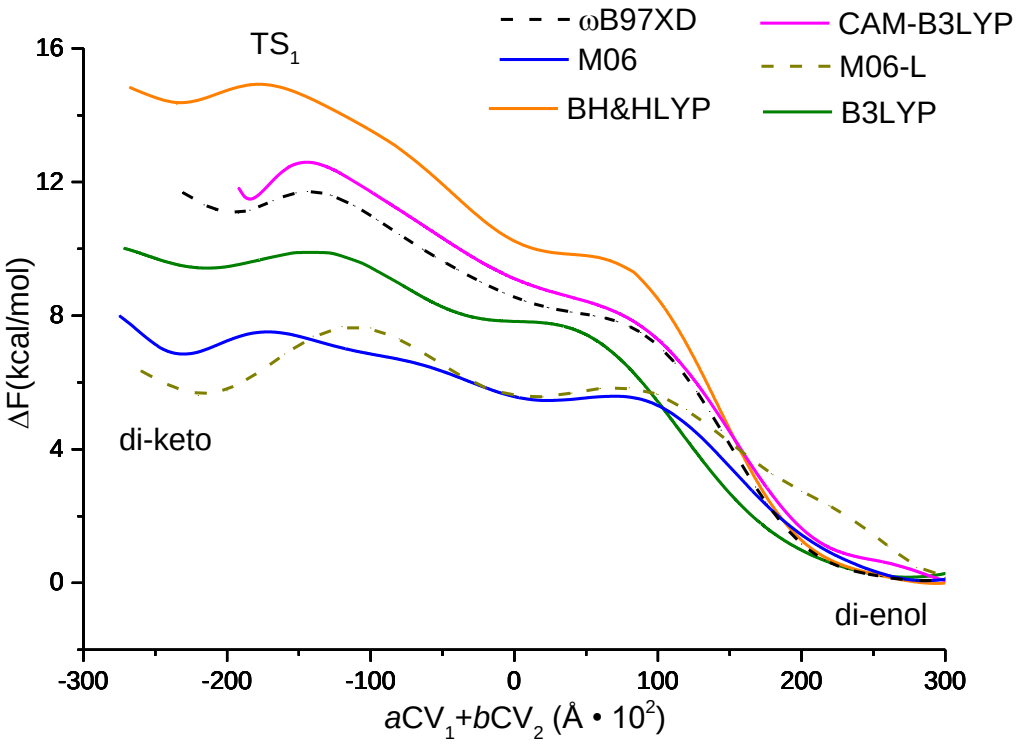
ωB97XD
M06
BH&HLYP
CAM-B3LYP
M06-L
B3LYP
TS1
ΔF(kcal/mol)
16
12
8
4
0
di-keto
di-enol
-300
-200
-100
0
100
200
300
aCV1+bCV2 (Å • 10^2)

Figure 7

Graphical Abstract

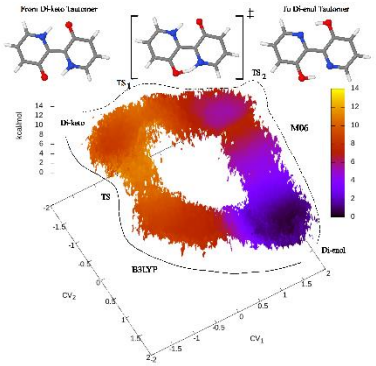

The description of the intramolecular double proton transfer in [2,2'-bipyridyl]-3-3'-diol depends on the selected exchange-correlation functional as suggested by the analysis carried out on the Potential and Free Energy Surfaces evaluated at DFT level.